The green tea catechin EGCG provides proof-of-concept for a pan-coronavirus entry inhibitor

Emmanuelle V. LeBlanc[1] and Che C. Colpitts[1,#]

[1]Department of Biomedical and Molecular Sciences, Queen's University, Kingston, ON K7L 3N6, Canada

[#]Correspondence: che.colpitts@queensu.ca

Abstract

The COVID-19 pandemic caused by the severe acute respiratory syndrome coronavirus-2 (SARS-CoV-2) has emphasized the serious threat to human health posed by emerging coronaviruses. Effective antiviral countermeasures are urgently needed as vaccine development and deployment against an emerging coronavirus takes time, even in the best-case scenario. The green tea catechin, epigallocatechin gallate (EGCG), has broad spectrum antiviral activity. We demonstrate here that EGCG prevents murine and human coronavirus infection and blocks the entry of lentiviral particles pseudotyped with spike proteins from highly pathogenic coronaviruses, as well as a bat coronavirus poised to emerge into humans. We show that EGCG treatment reduces coronavirus attachment to target cell surfaces. Our results demonstrate the potential for the development of pan-coronavirus attachment inhibitors to protect against current and future emerging coronaviruses.

Key words: SARS-CoV-2, coronavirus, entry inhibitor, natural product

24 **1. Introduction**

25 The novel severe acute respiratory syndrome coronavirus-2 (SARS-CoV-2) has infected hundreds
26 of millions of people and has resulted in millions of deaths around the world. The COVID-19
27 pandemic, caused by SARS-CoV-2, underscores the severe health threat posed by emerging
28 coronaviruses (CoVs), and makes evident the paucity of antivirals with extended spectrums of
29 activity. SARS-CoV-2 is the third highly pathogenic CoV to emerge in the 21st century. The
30 abundance and diversity of SARS-related CoVs in bats points to the likelihood of future spillover
31 into human populations (Li et al., 2005). In addition, seasonally circulating common cold CoVs
32 continually burden human health (Walsh et al., 2013), and cause severe disease in elderly
33 populations (Hand et al., 2018; Patrick et al., 2006), without effective preventative or therapeutic
34 strategies. In order to develop inhibitors that are effective against such a broad range of endemic,
35 pandemic, and emerging CoVs, a conserved step of viral infection needs to be targeted.

36 Most human viruses, including CoVs, initiate primary attachment to cell surfaces through
37 low-affinity but high-avidity interactions with glycans. Heparan sulfate proteoglycans are
38 necessary attachment receptors for the human alphacoronavirus NL63 (HCoV-NL63) (Milewska
39 et al., 2014), as well as many other human viruses, such as herpes simplex virus (HSV) (Lycke et
40 al., 1991; WuDunn and Spear, 1989), hepatitis C virus (HCV) (Germi et al., 2002; Morikawa et
41 al., 2007) and human immunodeficiency virus (HIV) (Patel et al., 1993). Recently, heparan sulfate
42 has also been identified as a necessary co-factor for SARS-CoV-2 infection (Clausen et al., 2020;
43 Zhang et al., 2020). Alternatively, other viruses, including influenza A virus (IAV) and
44 betacoronaviruses HCoV-OC43 and HCoV-HKU1 require sialic acid-containing glycans for
45 attachment and entry (Huang et al., 2015; Krempl et al., 1995; Weis et al., 1988). Regardless of
46 the glycan subtype, glycan binding is critical to the primary attachment of many different viruses,

47 facilitating their specific high-affinity interaction with less abundant protein receptors, such as
48 ACE2 for HCoV-NL63, SARS-CoV-1 and SARS-CoV-2 (Hoffmann et al., 2020; Hofmann et al.,
49 2005). For some viruses, like IAV, glycans serve as the only known entry receptor.

50 Blocking viral attachment to cellular glycans is a demonstrated approach to inhibit diverse
51 viral infections. Epigallocatechin gallate (EGCG) is the most bioactive polyphenolic compound
52 from green tea with antiviral activity against diverse DNA and RNA viruses, including HSV-1,
53 HCV, and IAV (Xu et al., 2017). The broad antiviral spectrum of EGCG has been attributed to its
54 ability to inhibit the primary attachment of unrelated viruses by competing with both heparan
55 sulfate and sialic acid for virion binding (Colpitts and Schang, 2014). However, whether EGCG
56 inhibits coronavirus infection by similar mechanisms remains unknown.

57 Here, we show that EGCG inhibits infectivity of murine, bat, and human CoVs. EGCG
58 blocks cell surface binding of multiple CoVs, suggesting that it inhibits a conserved step in CoV
59 attachment, such as initial binding to glycans. These findings demonstrate that blocking primary
60 attachment is a potential antiviral strategy to prevent infection by diverse CoVs.

61

62 **2. Material and Methods**

63 **2.1. Compounds**

64 Epigallocatechin-3-gallate (EGCG, 95% pure) was purchased from Thermo Fisher Scientific
65 (AC449010100). Heparin was obtained from Carbosynth Ltd (YH09354).

66

67 **2.2. Plasmids**

68 Lentiviral pseudoparticles were produced using plasmids encoding HIV-1 gag/pol (BEI Resources
69 NR-52517), tat (BEI Resources NR-52518), rev (BEI Resources NR-52519), a luciferase-

70 encoding lentiviral genome (BEI Resources NR-52516) and spike plasmids. The SARS-CoV-2
71 spike expression plasmid was obtained from Dr. Raffaele De Francesco (Addgene 155297). The
72 MERS-CoV spike expression plasmid was kindly provided by Dr. Stefan Pöhlmann (Göttingen,
73 Germany). The SARS-CoV-1 (Tor2 strain, GenBank accession no. **NC_004718.3**) and WIV1-
74 CoV spike (GenBank accession no. **KC881007.1**) expression plasmids were synthesized by
75 Genscript and codon-optimized for human expression. The lentiviral vector expressing human
76 ACE2 (Dr. Sonja Best, Addgene 154981) was used with the lentiviral packaging plasmid psPAX2
77 (Dr. Didier Trono, Addgene 12260) and pCMV-VSV-G (Dr. Bob Weinberg, Addgene 8454).
78

79 **2.3. Cells and viruses**

80 HEK293T/17 (ATCC CRL-11268), L929 (ATCC CCL-1), Huh7 (JCRB0403), HCT-8 (ATCC
81 CCL-244) and 17CL1 (BEI Resources NR-53719) cells were cultured in Dulbecco's minimal
82 essential medium (DMEM) with 10% FBS, 50 U/mL penicillin, and 50 µg/mL streptomycin at
83 37°C in 5% CO_2. A549 (BEI Resources NR-52268) cells were cultured in Hams F-12K (Kaighn's)
84 medium with 10% FBS, 50 U/mL penicillin, and 50 µg/mL streptomycin at 37°C in 5% CO_2. Calu-
85 3 (ATCC HTB-55) cells were cultured in minimal essential medium (MEM) with 10% FBS, 1 mM
86 sodium pyruvate, 1X non-essential amino acid solution, 50 U/mL penicillin, and 50 µg/mL
87 streptomycin at 37°C in 5% CO_2.

88 A549-ACE2 cells were generated by lentiviral transduction and selected with 10 µg/mL
89 blasticidin. The bulk population was single-cell cloned by limiting dilution, and ACE2 expression
90 of clonal populations was determined by Western blotting using a rabbit monoclonal ACE2
91 antibody (Invitrogen MA5-32307), mouse monoclonal actin (Abcam ab8226) or tubulin (Abcam
92 ab7291) antibodies, and a LICOR Odyssey CLx with appropriate secondary antibodies.

93 Human coronavirus 229E (HCoV-229E) and HCoV-OC43 were obtained from BEI
94 Resources (NR-52726 and NR-52725). For HCoV-229E, Huh7 cells were infected with a
95 multiplicity of infection (MOI) of 0.01 plaque-forming units (pfu)/cell and incubated at 33°C in
96 5% CO_2 until full cytopathic effects (CPE) were observed (∼5 days post-infection). The
97 supernatants were collected, and cellular debris was pelleted by centrifugation at 1,000 × g for 10
98 min. The resulting supernatant was then aliquoted, and the viral stocks were stored at −80°C. For
99 HCoV-OC43, HCT-8 cells were infected (MOI of 0.01) and incubated at 33°C in 5% CO_2 until
100 full CPE were observed (∼5 days post-infection). Similarly, supernatants were collected, cellular
101 debris was pelleted by centrifugation at 1,000 × g for 10 min and the resulting supernatant was
102 then aliquoted and stored at −80°C.
103 Green fluorescent protein-expressing murine hepatitis virus (MHV A59-GFP) was kindly
104 provided by Dr. Volker Thiel (Institute of Virology and Immunology, Bern, Switzerland) (Coley
105 et al., 2005). VSV-SARS-CoV-2 S was a gift from Dr. Sean Whelan (Washington University
106 School of Medicine in St. Louis, USA) (Case et al., 2020). MHV A59-GFP and VSV-SARS-CoV-
107 2 were propagated as described (Coley et al., 2005; Case et al., 2020).
108
109 **2.4. Infectivity assays**
110 Huh7 cells (1.6 × 10^6 cells/well in 6-well plates) were infected with approximately 100 PFU of
111 HCoV-229E pre-exposed for 10 min at 37°C to EGCG or dimethyl sulfoxide (DMSO) vehicle in
112 DMEM. Inocula were removed 2 h later, and monolayers were overlaid with 1.2%
113 carboxymethylcellulose (Fisher Scientific AAA1810536) in DMEM containing 2% FBS. Infected
114 cells were incubated at 33°C in 5% CO_2 until 4 days post-infection, when they were fixed with

115 10% formalin and stained with 1% (wt/vol) crystal violet–10% (vol/vol) ethanol in H_2O for
116 counting plaques.

117 Huh7 and A549 cells (4×10^5 cells/well in 24-well plates) were infected with
118 approximately 200 focus-forming units (FFU) of HCoV-OC43, pre-exposed to EGCG or DMSO
119 vehicle for 10 min at 37°C in DMEM. Inocula were removed 2 h later, and monolayers were
120 overlaid with 1.2% microcrystalline colloidal cellulose (Sigma-Aldrich 435244) in DMEM
121 containing 2% FBS. Infected cells were incubated at 33°C in 5% CO_2 for 3 days, then fixed and
122 processed for immunofluorescence to detect OC43 nucleoprotein. Cells were incubated with
123 primary mouse IgG anti-coronavirus group antibody MAB9013 (Millipore Sigma; diluted 1:500)
124 for 1 h at room temperature, followed by addition of secondary Alexa Fluor 488 anti-mouse IgG
125 Fab 2 antibody (Cell Signaling Technology 4408S) for 1 h at room temperature. Foci were
126 visualized and counted under a fluorescence microscope (Nikon Eclipse Ts2).

127 MHV A59-GFP virions pre-exposed to EGCG or the DMSO vehicle control for 10 min at
128 37°C in DMEM were used to infect L929 cell monolayers. Inocula were removed 1 h later, and
129 monolayers were overlaid with 1.2% carboxymethylcellulose in DMEM containing 2% FBS.
130 Infected cells were incubated at 33°C in 5% CO_2 for 24 h, then fixed prior to counting of GFP-
131 positive cells under the fluorescence microscope.

132 VSV-SARS-CoV-2 S virions pre-exposed to EGCG or the DMSO vehicle control for 10
133 min at 37°C in DMEM were used to infect Huh7, A549-ACE2 or Calu-3 cell monolayers in
134 duplicate wells of a 96-well plate. Infected cells were incubated at 33°C in 5% CO_2 for 24 h, then
135 fixed with 10% formalin. GFP signals were captured by Nikon Eclipse Ts2, processed using the
136 Python Imaging Library to find the mean grey value, and plotted as percentage of inhibition.

137 In all experiments, half maximal inhibitory concentrations (IC_{50}) were calculated by
138 nonlinear regression analysis using GraphPad Prism (version 9.0; GraphPad Software, Inc.).
139
140 **2.5. Pseudoparticle entry assays**
141 Lentiviral pseudoparticles were generated in HEK293T/17 cells by co-transfection using
142 Lipofectamine 2000 (Invitrogen 11668-019) (Crawford et al., 2020). The CoV spike expression
143 plasmids were co-transfected with a luciferase-encoding lentiviral genome, and plasmids encoding
144 HIV-1 gag/pol, tat, and rev (Crawford et al., 2020). Cell culture supernatants containing
145 coronavirus spike pseudotyped lentiviral particles were collected at 48 and 72 hours post-
146 transfection, pooled and filtered through a 0.45 μm filter, and stored at -80°C.
147 Pseudoparticles were incubated for 10 min at 37°C with serially diluted EGCG and used
148 to infect Huh7 or A549-ACE2 cells in triplicate in 96-well plates. Infectivity was determined after
149 3 days by luminescence following addition of BrightGlo reagent (Promega PR-E2620). IC_{50} were
150 calculated by nonlinear regression analysis using GraphPad Prism (version 9.0; GraphPad
151 Software, Inc.).
152
153 **2.6.Cell toxicity assay**
154 Cells (50,000 per well in 96-well plate) were treated with EGCG or DMSO in DMEM and
155 incubated at 37°C in 5% CO_2 for 2h. To mimic the conditions used in the infectivity and
156 pseudoparticle assays, media was removed, cells were washed with PBS, and supplemented with
157 normal culture media of DMEM with 10% FBS, 50 U/mL penicillin, and 50 μg/mL streptomycin.
158 After 72 h, cell viability was assessed using alamarBlue cell viability reagent (Invitrogen
159 DAL1025) on a fluorescence plate reader (SpectraMax ID3 Multimode Plate reader).

160

161 **2.7. Time-of-addition experiments**

162 Near-confluent Huh7 and A549 cell monolayers in 12 or 24-well plates were pre-treated with
163 EGCG or DMSO vehicle for 1 h at 37°C in DMEM. Cells were washed with DMEM and infected
164 with 50-200 PFU of HCoV-229E or HCoV-OC43 for 2 h at 33°C. Alternatively, Huh7 and A549
165 cells were first infected with HCoV-229E or HCoV-OC43 for 2 h at 33°C. After removing the
166 inocula, the infected cells were overlaid with 1.2% microcrystalline colloidal cellulose in DMEM-
167 2% FBS containing EGCG or DMSO. Infectivity was assessed by plaquing efficiency or
168 immunostaining.

169

170 **2.8. Binding assays**

171 OC43 (4 x 10^4 PFU; MOI 0.05) or VSV-SARS-CoV-2 (2 x 10^5 PFU; MOI 0.5, chosen to match
172 the conditions of the infectivity assay) were exposed for 10 min at 37°C to EGCG or DMSO in
173 DMEM and adsorbed onto pre-chilled Huh7 and A549 cells for 1 h at 4°C. After three washes
174 with cold phosphate-buffered saline (PBS), cells were lysed and RNA was isolated using the
175 Monarch Total RNA Miniprep Kit (NEB T2010S), according to the manufacturer's instructions.
176 The RNA was transcribed to cDNA using the High Capacity cDNA Reverse Transcription Kit
177 (Applied Biosystems LS4368814). Quantitative real-time PCR was performed on the QuantStudio
178 3 (Applied Biosystems) instrument, using PowerTrack SYBR Green Master Mix (Applied
179 Biosystems LSA46110), with primers to detect actin (F: 5'-CTGGGAGTGGGTGGAGGC-3', R:
180 5'-TCAACTGGTCTCAAGTCAGTG-3') and OC43 N gene (F: 5'-
181 CCCAAGCAAACTGCTACCTCTCAG-3', R: 5'-GTAGACTCCGTCAATATCGGTGCC-3')
182 or VSV N gene (F: 5'-GATAGTACCGGAGGATTGACGACTA-3', R: 5'-

183 TCAAACCATCCGAGCCATTC-3'). Following normalization to actin, the percentage of binding
184 was expressed relative to binding of virions treated with the DMSO control.
185
186 **3. Results**
187 **3.1. EGCG inhibits murine and human coronavirus infection**
188 We first tested the effect of EGCG on the infectivity of human common cold CoVs HCoV-229E
189 (an alphacoronavirus) and HCoV-OC43 (a betacoronavirus). HCoV-229E and HCoV-OC43
190 virions were treated with DMSO or varying concentrations of EGCG for 10 min at 37°C and used
191 to inoculate infection-susceptible human hepatoma Huh7 or human lung epithelial A549 cell
192 monolayers. After 2 h of infection, inocula were removed and cells were overlaid with plaquing
193 media. Infectivity was assessed by plaquing efficiency on Huh7 for HCoV-229E or by
194 immunofluorescence focus-forming assay on Huh7 and A549 cells for HCoV-OC43. EGCG
195 inhibited infectivity of HCoV-229E (IC_{50} = 0.77 μM) and HCoV-OC43 (IC_{50} = 0.49-0.56 μM) at
196 sub- to low micromolar concentrations (**Figure 1A**), similar to other viruses highly susceptible to
197 inhibition by EGCG, such as HSV-1 (Colpitts and Schang, 2014). We next tested the inhibitory
198 activity of EGCG against a murine CoV, murine hepatitis virus (MHV-A59), on murine fibroblast
199 L929 cell monolayers. EGCG inhibited MHV-A59 infection with similar potency as for the human
200 common cold CoVs (IC_{50} = 0.71 μM) (**Figure 1B**) and inhibited the formation of syncytia (**Figure**
201 **1C**). Consistent with previous reports, we found EGCG to have minimal effect on cell viability at
202 the low micromolar range in which antiviral activity is exerted (**Figure 1D**).
203
204 **3.2. EGCG inhibits entry of highly pathogenic and emerging coronaviruses**

205 We produced luciferase-encoding lentiviral particles pseudotyped with SARS-CoV-1, SARS-
206 CoV-2 and MERS-CoV spike (S) proteins to investigate the effect of EGCG on entry of highly
207 pathogenic CoVs. We also generated lentiviral particles pseudotyped with the spike protein of
208 WIV1-CoV, a bat CoV that binds to human ACE2 (Ge et al., 2013). Huh7 cells were incubated
209 with CoV S pseudoparticles pre-exposed to EGCG or DMSO for 10 min at 37°C. Inocula were
210 removed after 2 h and replaced with fresh DMEM. After 72 h, cells were lysed and luminescence
211 was measured. EGCG inhibited SARS-CoV-1, SARS-CoV-2, MERS-CoV and WIV1-CoV
212 pseudoparticle entry with IC_{50} of 2.5, 48.6, 13.7 and 3.8 μM, respectively (**Figure 2A**). We also
213 generated A549 human lung alveolar epithelial cells stably expressing human ACE2, the receptor
214 for SARS-CoV-1 and SARS-CoV-2, and isolated a clone with high levels of ACE2 expression and
215 enhanced susceptibility to SARS-CoV-2 S pseudoparticle infection (**Supplemental Figure 1**).
216 EGCG similarly inhibited entry of SARS-CoV-1, SARS-CoV-2, and WIV1-CoV pseudoparticles
217 into A549-ACE2 B9 cells, with IC_{50} of 15.9, 24.0 and 24.5 μM, respectively (**Figure 2A**).
218 We assessed the effect of EGCG on replication-competent vesicular stomatitis virus (VSV)
219 virions expressing GFP and SARS-CoV-2 S instead of the VSV glycoprotein (VSV-SARS-CoV-
220 2) (Case et al., 2020). Huh7, A549-ACE2, and lung epithelial Calu-3 cells were infected with
221 EGCG-treated VSV-SARS-CoV-2 virions (MOI of 5). Infected cells were imaged by fluorescence
222 microscopy after 24 h. Similar to the pseudoparticle assays, EGCG inhibited VSV-SARS-CoV-2
223 S infection with IC_{50} ranging from 11.45 to 15.40 μM, depending on the cell type (**Figure 2B**),
224 with minimal cytotoxicity up to 100 μM (**Supplemental Figure 2**). We next evaluated whether
225 the effect of EGCG was dependent on MOI. Using the same assay, but with MOI of 0.5, we found
226 that EGCG inhibited VSV-SARS-CoV-2 infection with IC_{50} ranging from 0.14 to 1.13 μM. These
227 findings demonstrate that the inhibitory activity of EGCG depends on the MOI (**Figure 2B**),

228 consistent with the virions as the proposed target of EGCG (Colpitts and Schang, 2014). This also
229 provides a potential explanation for the difference in IC_{50} for authentic viruses investigated at low
230 MOI (<0.001) (**Figure 1A-B**) compared to lentiviral pseudoparticles (**Figure 2A**). Based on p24
231 ELISA data for lentiviral particles pseudotyped with SARS-CoV-2 spike in our laboratory, we
232 estimate lentiviral titers of approximately 1.7 x 10^6 transducing units/mL, resulting in an apparent
233 MOI of 3.4 in these experiments.
234
235 **3.3. EGCG acts on virions to inhibit coronavirus binding to cell surfaces**
236 To confirm that EGCG acts on CoV virions, and not on cells, we performed time-of-addition
237 experiments. Cells were pre-treated with EGCG or DMSO 1 h at 37°C, at which point media was
238 removed and cells were infected with HCoV-229E or HCoV-OC43. Alternatively, cells were
239 infected, and EGCG- or DMSO-containing medium was added at 2 h post-infection. Infectivity
240 was determined by plaque assay or immunostaining. In either condition, no inhibition of infectivity
241 was observed until the highest concentration of 100 μM EGCG (**Figure 3A**), consistent with the
242 main effect of EGCG being on viral entry, with virions as the target. To test if EGCG inhibits CoV
243 attachment, we performed binding assays in which cells were incubated with pre-treated virions at
244 4°C for 1 h to allow for attachment, but not fusion or entry. After cell washing, bound virions were
245 quantified by RT-qPCR (**Supplemental Figure 3**). Pre-chilled Huh7 or Calu-3 cells were
246 inoculated with HCoV-OC43 or VSV-SARS-CoV-2 treated with DMSO, 10 μM EGCG, or 20
247 μg/mL heparin, as a control attachment inhibitor (Clausen et al., 2020). As expected, heparin
248 partially blocked VSV-SARS-CoV-2 binding. We also observed that heparin reduced HCoV-
249 OC43 binding, which unlike other coronavirus does not have a known protein receptor but depends
250 on sialic acid, and, as recently reported, glycosaminoglycans for entry (Wang et al., 2021). EGCG

251 similarly reduced HCoV-OC43 and VSV-SARS-CoV-2 binding to Huh7 and Calu-3 cells (**Figure**
252 **3B-C**).
253
254 **4. Discussion**
255 Green tea catechins, especially EGCG, exert antiviral effects against diverse viruses. We show that
256 EGCG broadly inhibits CoV infections, and that its activity is due, at least in part, to blocking CoV
257 attachment to target cells. Infection by authentic murine and human CoVs, as well as entry of
258 lentivirus particles pseudotyped with spike proteins of highly pathogenic or potentially emerging
259 CoVs (Ge et al., 2013), was inhibited by EGCG treatment. Interestingly, EGCG was recently
260 shown to significantly inhibit authentic SARS-CoV-2 infection, and time-of-addition experiments
261 suggested that EGCG at least partially blocks SARS-CoV-2 entry (Henss et al., 2021), consistent
262 with our findings. Here, we expand the scope of EGCG activity to other CoVs, including murine
263 and bat CoVs, and demonstrate that EGCG inhibits CoV attachment and infection of lung epithelial
264 cell lines.
265 A variety of mechanisms for the antiviral activity of EGCG have been described. EGCG
266 inhibits the primary attachment of diverse viruses including VSV, IAV, HCV, HSV-1 and vaccinia
267 virus (Colpitts and Schang, 2014). EGCG is proposed to act directly on HCV virions to block
268 attachment in a genotype independent manner, with no alteration in HCV (co)-receptor expression
269 nor any effect on viral replication, assembly, or release (Calland et al., 2012; Ciesek et al., 2011).
270 For HBV, EGCG may inhibit entry (Huang et al., 2014), as well as replication, with proposed roles
271 in impairing HBV replicative intermediates during DNA synthesis (He et al., 2011), diminishing
272 the transcriptional activation of the HBV core promoter (Xu et al., 2016), and enhancing lysosomal
273 acidification to adversely affect HBV replication (Zhong et al., 2015). EGCG is suggested to

274 prevent the binding of HIV glycoprotein 120 to its receptor molecule CD4 on cells (Williamson et
275 al., 2006), and to act as an HIV reverse transcriptase inhibitor (Li et al., 2011). Finally, recent
276 studies have identified *in vitro* inhibitory effects of EGCG against the SARS-CoV-2 3C-like
277 protease (Chiou et al., 2021; Du et al., 2021; Jang et al., 2021, 2020). However, our time-of-
278 addition experiments with HCoV-229E and HCoV-OC43, as well as those of others with SARS-
279 CoV-2 (Henss et al., 2021), strongly suggest that EGCG predominantly inhibits authentic CoV
280 infection by blocking entry, although other antiviral activities might be exerted at higher
281 concentrations. Furthermore, we show that EGCG reduces cell surface binding of HCoV-OC43
282 and VSV-SARS-CoV-2, in a similar manner to heparin, which has been demonstrated to
283 competitively block virion attachment (Clausen et al., 2020).

284 While COVID-19 vaccine development and deployment are ongoing, extensive efforts are
285 underway to identify antibodies, peptides, and small molecules to prevent SARS-CoV-2 entry (Xiu
286 et al., 2020). To protect against emerging CoVs, the identification of broad-spectrum entry
287 inhibitors is a priority. Recently, lactoferrins have been described to disrupt CoV primary
288 attachment, mediated by heparan sulfate interactions, conferring antiviral activity against multiple
289 CoVs *in vitro*, demonstrating the potential for a pan-coronavirus inhibitor (Hu et al., 2021). Small
290 molecules continue to be preferred as drugs in general due to superior pharmacokinetic properties
291 and simpler synthesis (Ngo and Garneau-Tsodikova, 2018). As with other green tea catechins,
292 EGCG does not accumulate at high levels, is unstable under physiological conditions, and is
293 rapidly metabolized (Chow et al., 2003; Lambert et al., 2003; Smith, 2011). However, the
294 observation that a small molecule exerts pan-coronavirus activity provides the basis for the
295 development of entry inhibitors that could provide an effective antiviral strategy to protect against
296 future emerging CoV infections.

Funding information

This work was supported by a Natural Sciences and Engineering Research Council of Canada Discovery Grant, a Banting Research Foundation Discovery Award, as well as by the Canadian Foundation for Innovation John R. Evans Leaders Fund, and Queen's University. E.V.L. is supported by a Vanier Canada Graduate Scholarship.

Acknowledgements

The following reagents were obtained through BEI Resources (NIAID, NIH): *Homo sapiens* A549 Lung Carcinoma Cells (NR-52268); Murine 17CL1 Cell Line (NR-53719); SARS-Related Coronavirus 2, Wuhan-Hu-1 Spike-Pseudotyped Lentiviral Kit (NR-52948); Human Coronavirus OC43 (NR-52725) and 229E (NR-52726). We thank Gerard O'Leary for Python processing scripts, Dr. Selena Sagan (McGill University) for providing coronavirus infection protocols, and Dr. Chantelle Capicciotti (Queen's University) for helpful discussions.

References

Calland, N., Albecka, A., Belouzard, S., Wychowski, C., Duverlie, G., Descamps, V., Hober, D., Dubuisson, J., Rouillé, Y., Séron, K., 2012. (−)-Epigallocatechin-3-gallate is a new inhibitor of hepatitis C virus entry. Hepatology 55, 720–729. https://doi.org/10.1002/hep.24803

Case, J.B., Rothlauf, P.W., Chen, R.E., Liu, Z., Zhao, H., Kim, A.S., Bloyet, L.-M., Zeng, Q., Tahan, S., Droit, L., Ilagan, M.X.G., Tartell, M.A., Amarasinghe, G., Henderson, J.P., Miersch, S., Ustav, M., Sidhu, S., Virgin, H.W., Wang, D., Ding, S., Corti, D., Theel, E.S., Fremont, D.H., Diamond, M.S., Whelan, S.P.J., 2020. Neutralizing Antibody and Soluble

320 ACE2 Inhibition of a Replication-Competent VSV-SARS-CoV-2 and a Clinical Isolate of
321 SARS-CoV-2. Cell Host Microbe 28, 475-485.e5.
322 https://doi.org/10.1016/j.chom.2020.06.021
323 Chiou, W.-C., Chen, J.-C., Chen, Y.-T., Yang, J.-M., Hwang, L.-H., Lyu, Y.-S., Yang, H.-Y.,
324 Huang, C., 2021. The inhibitory effects of PGG and EGCG against the SARS-CoV-2 3C-
325 like protease. Biochem. Biophys. Res. Commun. S0006-291X, 32299–3.
326 https://doi.org/10.1016/j.bbrc.2020.12.106
327 Chow, H.-H.S., Cai, Y., Hakim, I.A., Crowell, J.A., Shahi, F., Brooks, C.A., Dorr, R.T., Hara,
328 Y., Alberts, D.S., 2003. Pharmacokinetics and Safety of Green Tea Polyphenols after
329 Multiple-Dose Administration of Epigallocatechin Gallate and Polyphenon E in Healthy
330 Individuals. Clin. Cancer Res. 9, 3312–3319.
331 Ciesek, S., von Hahn, T., Colpitts, C.C., Schang, L.M., Friesland, M., Steinmann, J., Manns,
332 M.P., Ott, M., Wedemeyer, H., Meuleman, P., Pietschmann, T., Steinmann, E., 2011. The
333 green tea polyphenol, epigallocatechin-3-gallate, inhibits hepatitis C virus entry.
334 Hepatology 54, 1947–1955. https://doi.org/10.1002/hep.24610
335 Clausen, T.M., Sandoval, D.R., Spliid, C.B., Pihl, J., Perrett, H.R., Painter, C.D., Narayanan, A.,
336 Majowicz, S.A., Kwong, E.M., McVicar, R.N., Thacker, B.E., Glass, C.A., Yang, Z.,
337 Torres, J.L., Golden, G.J., Bartels, P.L., Porell, R., Garretson, A.F., Laubach, L., Feldman,
338 J., Yin, X., Pu, Y., Hauser, B., Caradonna, T.M., Kellman, B.P., Martino, C., Gordts,
339 P.L.S.M., Chanda, S.K., Schmidt, A.G., Godula, K., Leibel, S.L., Jose, J., Corbett, K.D.,
340 Ward, A.B., Carlin, A.F., Esko, J.D., 2020. SARS-CoV-2 Infection Depends on Cellular
341 Heparan Sulfate and ACE2. Cell 183, 1043-1057.e15.
342 https://doi.org/10.1016/j.cell.2020.09.033

343 Coley, S.E., Lavi, E., Sawicki, S.G., Fu, L., Schelle, B., Karl, N., Siddell, S.G., Thiel, V., 2005.
344 Recombinant mouse hepatitis virus strain A59 from cloned, full-length cDNA replicates to
345 high titers in vitro and is fully pathogenic in vivo. J. Virol. 79, 3097–3106.
346 https://doi.org/10.1128/JVI.79.5.3097-3106.2005
347 Colpitts, C.C., Schang, L.M., 2014. A Small Molecule Inhibits Virion Attachment to Heparan
348 Sulfate- or Sialic Acid-Containing Glycans. J. Virol. 88, 7806–7817.
349 https://doi.org/10.1128/JVI.00896-14
350 Crawford, K.H.D., Eguia, R., Dingens, A.S., Loes, A.N., Malone, K.D., Wolf, C.R., Chu, H.Y.,
351 Tortorici, M.A., Veesler, D., Murphy, M., Pettie, D., King, N.P., Balazs, A.B., Bloom, J.D.,
352 2020. Protocol and Reagents for Pseudotyping Lentiviral Particles with SARS-CoV-2 Spike
353 Protein for Neutralization Assays. Viruses. https://doi.org/10.3390/v12050513
354 Du, A., Zheng, R., Disoma, C., Li, Shiqin, Chen, Z., Li, Sijia, Liu, P., Zhou, Y., Shen, Y., Liu,
355 S., Zhang, Y., Dong, Z., Yang, Q., Alsaadawe, M., Razzaq, A., Peng, Y., Chen, X., Hu, L.,
356 Peng, J., Zhang, Q., Jiang, T., Mo, L., Li, Shanni, Xia, Z., 2021. Epigallocatechin-3-gallate,
357 an active ingredient of Traditional Chinese Medicines, inhibits the 3CLpro activity of
358 SARS-CoV-2. Int. J. Biol. Macromol. 176, 1–12.
359 https://doi.org/10.1016/j.ijbiomac.2021.02.012
360 Ge, X.-Y., Li, J.-L., Yang, X.-L., Chmura, A.A., Zhu, G., Epstein, J.H., Mazet, J.K., Hu, B.,
361 Zhang, W., Peng, C., Zhang, Y.-J., Luo, C.-M., Tan, B., Wang, N., Zhu, Y., Crameri, G.,
362 Zhang, S.-Y., Wang, L.-F., Daszak, P., Shi, Z.-L., 2013. Isolation and characterization of a
363 bat SARS-like coronavirus that uses the ACE2 receptor. Nature 503, 535–538.
364 https://doi.org/10.1038/nature12711
365 Germi, R., Crance, J.-M., Garin, D., Guimet, J., Lortat-Jacob, H., Ruigrok, R.W.H., Zarski, J.-P.,

366 Drouet, E., 2002. Cellular glycosaminoglycans and low density lipoprotein receptor are
367 involved in hepatitis C virus adsorption. J. Med. Virol. 68, 206–215.
368 https://doi.org/10.1002/jmv.10196
369 Hand, J., Rose, E.B., Salinas, A., Lu, X., Sakthivel, S.K., Schneider, E., Watson, J.T., 2018.
370 Severe respiratory illness outbreak associated with human coronavirus NL63 in a long-term
371 care facility. Emerg. Infect. Dis. https://doi.org/10.3201/eid2410.180862
372 He, W., Li, L.X., Liao, Q.J., Liu, C.L., Chen, X.L., 2011. Epigallocatechin gallate inhibits HBV
373 DNA synthesis in a viral replication - inducible cell line. World J. Gastroenterol. 17, 1507–
374 1514. https://doi.org/10.3748/wjg.v17.i11.1507
375 Henss, L., Auste, A., Schürmann, C., Schmidt, C., von Rhein, C., Mühlebach, M.D., Schnierle,
376 B.S., 2021. The green tea catechin epigallocatechin gallate inhibits SARS-CoV-2 infection.
377 J. Gen. Virol. 102. https://doi.org/10.1099/jgv.0.001574
378 Hoffmann, M., Kleine-Weber, H., Schroeder, S., Krüger, N., Herrler, T., Erichsen, S.,
379 Schiergens, T.S., Herrler, G., Wu, N.-H., Nitsche, A., Müller, M.A., Drosten, C., Pöhlmann,
380 S., 2020. SARS-CoV-2 Cell Entry Depends on ACE2 and TMPRSS2 and Is Blocked by a
381 Clinically Proven Protease Inhibitor. Cell 181, 271-280.e8.
382 https://doi.org/10.1016/j.cell.2020.02.052
383 Hofmann, H., Pyrc, K., van der Hoek, L., Geier, M., Berkhout, B., Pöhlmann, S., 2005. Human
384 coronavirus NL63 employs the severe acute respiratory syndrome coronavirus receptor for
385 cellular entry. Proc. Natl. Acad. Sci. 102, 7988–7993.
386 https://doi.org/10.1073/pnas.0409465102
387 Hu, Y., Meng, X., Zhang, F., Xiang, Y., Wang, J., 2021. The in vitro antiviral activity of
388 lactoferrin against common human coronaviruses and SARS-CoV-2 is mediated by

389 targeting the heparan sulfate co-receptor. Emerg. Microbes Infect. 10, 317–330.
390 https://doi.org/10.1080/22221751.2021.1888660
391 Huang, H.-C., Tao, M.-H., Hung, T.-M., Chen, J.-C., Lin, Z.-J., Huang, C., 2014. (−)-
392 Epigallocatechin-3-gallate inhibits entry of hepatitis B virus into hepatocytes. Antiviral Res.
393 111, 100–111. https://doi.org/10.1016/j.antiviral.2014.09.009
394 Huang, X., Dong, W., Milewska, A., Golda, A., Qi, Y., Zhu, Q.K., Marasco, W.A., Baric, R.S.,
395 Sims, A.C., Pyrc, K., Li, W., Sui, J., 2015. Human Coronavirus HKU1 Spike Protein Uses
396 O -Acetylated Sialic Acid as an Attachment Receptor Determinant and Employs
397 Hemagglutinin-Esterase Protein as a Receptor-Destroying Enzyme. J. Virol. 89, 7202–13.
398 https://doi.org/10.1128/jvi.00854-15
399 Jang, M., Park, R., Park, Y.-I., Cha, Y.-E., Yamamoto, A., Lee, J.I., Park, J., 2021. EGCG, a
400 green tea polyphenol, inhibits human coronavirus replication in vitro. Biochem. Biophys.
401 Res. Commun. 547, 23–28. https://doi.org/10.1016/j.bbrc.2021.02.016
402 Jang, M., Park, Y.-I., Cha, Y.-E., Park, R., Namkoong, S., Lee, J.I., Park, J., 2020. Tea
403 Polyphenols EGCG and Theaflavin Inhibit the Activity of SARS-CoV-2 3CL-Protease *In*
404 *Vitro*. Evidence-Based Complement. Altern. Med. 2020, 5630838.
405 https://doi.org/10.1155/2020/5630838
406 Krempl, C., Schultze, B., Herrler, G., 1995. Analysis of cellular receptors for human coronavirus
407 OC43, in: Advances in Experimental Medicine and Biology. pp. 371–4.
408 https://doi.org/10.1007/978-1-4615-1899-0_60
409 Lambert, J.D., Lee, M.-J., Lu, H., Meng, X., Hong, J.J.J., Seril, D.N., Sturgill, M.G., Yang, C.S.,
410 2003. Epigallocatechin-3-Gallate Is Absorbed but Extensively Glucuronidated Following
411 Oral Administration to Mice. J. Nutr. 133, 4172–4177.

412 https://doi.org/10.1093/jn/133.12.4172
413 Li, S., Hattori, T., Kodama, E.N., 2011. Epigallocatechin gallate inhibits the HIV reverse
414 transcription step. Antivir. Chem. Chemother. 21, 239–243.
415 https://doi.org/10.3851/IMP1774
416 Li, W., Shi, Z., Yu, M., Ren, W., Smith, C., Epstein, J.H., Wang, H., Crameri, G., Hu, Z., Zhang,
417 H., Zhang, J., McEachern, J., Field, H., Daszak, P., Eaton, B.T., Zhang, S., Wang, L.-F.,
418 2005. Bats Are Natural Reservoirs of SARS-Like Coronaviruses. Science (80-.). 310, 676–
419 679. https://doi.org/10.1126/science.1118391
420 Lycke, E., Johansson, M., Svennerholm, B., Lindahl, U., 1991. Binding of herpes simplex virus
421 to cellular heparan sulphate, an initial step in the adsorption process. J. Gen. Virol. 72,
422 1131–1137. https://doi.org/10.1099/0022-1317-72-5-1131
423 Milewska, A., Zarebski, M., Nowak, P., Stozek, K., Potempa, J., Pyrc, K., 2014. Human
424 coronavirus NL63 utilizes heparan sulfate proteoglycans for attachment to target cells. J.
425 Virol. 88, 13221–13230. https://doi.org/10.1128/JVI.02078-14
426 Millet, J.K., Whittaker, G.R., 2016. Murine Leukemia Virus (MLV)-based Coronavirus Spike-
427 pseudotyped Particle Production and Infection. Bio Protoc 6, e2035.
428 https://doi.org/https://doi-org.myaccess.library.utoronto.ca/10.21769/BioProtoc.2035
429 Morikawa, K., Zhao, Z., Date, T., Miyamoto, M., Murayama, A., Akazawa, D., Tanabe, J., Sone,
430 S., Wakita, T., 2007. The roles of CD81 and glycosaminoglycans in the adsorption and
431 uptake of infectious HCV particles. J. Med. Virol. 79, 714–723.
432 https://doi.org/10.1002/jmv.20842
433 Ngo, H.X., Garneau-Tsodikova, S., 2018. What are the drugs of the future? Medchemcomm 9,
434 757–758. https://doi.org/10.1039/c8md90019a

435 Patel, M., Yanagishita, M., Roderiquez, G., Bou-Habib, D.C., Oravecz, T., Hascall, V.C.,
436 Norcorss, M.A., 1993. Cell-Surface Heparan Sulfate Proteoglycan Mediates HIV-1
437 Infection of T-Cell Lines. AIDS Res. Hum. Retroviruses 9, 167–174.
438 https://doi.org/10.1089/aid.1993.9.167
439 Patrick, D.M., Petric, M., Skowronski, D.M., Guasparini, R., Booth, T.F., Krajden, M., McGeer,
440 P., Bastien, N., Gustafson, L., Dubord, J., Macdonald, D., David, S.T., Srour, L.F., Parker,
441 R., Andonov, A., Isaac-Renton, J., Loewen, N., McNabb, G., McNabb, A., Goh, S.-H.,
442 Henwick, S., Astell, C., Guo, J.P., Drebot, M., Tellier, R., Plummer, F., Brunham, R.C.,
443 2006. An Outbreak of Human Coronavirus OC43 Infection and Serological Cross-reactivity
444 with SARS Coronavirus. Can. J. Infect. Dis. Med. Microbiol. 17, 330–336.
445 https://doi.org/10.1155/2006/152612
446 Smith, T.J., 2011. Green tea polyphenols in drug discovery: a success or failure? Expert Opin.
447 Drug Discov. 6, 589–595. https://doi.org/10.1517/17460441.2011.570750
448 Walsh, E.E., Shin, J.H., Falsey, A.R., 2013. Clinical impact of human coronaviruses 229E and
449 OC43 infection in diverse adult populations. J. Infect. Dis. 208, 1634–1642.
450 https://doi.org/10.1093/infdis/jit393
451 Wang, R., Simoneau, C.R., Kulsuptrakul, J., Bouhaddou, M., Travisano, K.A., Hayashi, J.M.,
452 Carlson-Stevermer, J., Zengel, J.R., Richards, C.M., Fozouni, P., Oki, J., Rodriguez, L.,
453 Joehnk, B., Walcott, K., Holden, K., Sil, A., Carette, J.E., Krogan, N.J., Ott, M., Puschnik,
454 A.S., 2021. Genetic Screens Identify Host Factors for SARS-CoV-2 and Common Cold
455 Coronaviruses. Cell 184, 106-119.e14. https://doi.org/10.1016/j.cell.2020.12.004
456 Weis, W., Brown, J.H., Cusack, S., Paulson, J.C., Skehel, J.J., Wiley, D.C., 1988. Structure of
457 the influenza virus haemagglutinin complexed with its receptor, sialic acid. Nature 333,

458 426–431. https://doi.org/10.1038/333426a0
459 Williamson, M.P., McCormick, T.G., Nance, C.L., Shearer, W.T., 2006. Epigallocatechin
460 gallate, the main polyphenol in green tea, binds to the T-cell receptor, CD4: Potential for
461 HIV-1 therapy. J. Allergy Clin. Immunol. 118, 1369–1374.
462 https://doi.org/10.1016/j.jaci.2006.08.016
463 WuDunn, D., Spear, P.G., 1989. Initial interaction of herpes simplex virus with cells is binding
464 to heparan sulfate. J. Virol. 63, 52–58. https://doi.org/10.1128/JVI.63.1.52-58.1989
465 Xiu, S., Dick, A., Ju, H., Mirzaie, S., Abdi, F., Cocklin, S., Zhan, P., Liu, X., 2020. Inhibitors of
466 SARS-CoV-2 Entry: Current and Future Opportunities. J. Med. Chem. 63, 12256–12274.
467 https://doi.org/10.1021/acs.jmedchem.0c00502
468 Xu, J., Gu, W., Li, C., Li, X., Xing, G., Li, Y., Song, Y., Zheng, W., 2016. Epigallocatechin
469 gallate inhibits hepatitis B virus via farnesoid X receptor alpha. J. Nat. Med. 70, 584–591.
470 https://doi.org/10.1007/s11418-016-0980-6
471 Xu, J., Xu, Z., Zheng, W., 2017. A Review of the Antiviral Role of Green Tea Catechins.
472 Molecules 22, 1337. https://doi.org/10.3390/molecules22081337
473 Zhang, Q., Chen, C.Z., Swaroop, M., Xu, M., Wang, L., Lee, J., Wang, A.Q., Pradhan, M.,
474 Hagen, N., Chen, L., Shen, M., Luo, Z., Xu, X., Xu, Y., Huang, W., Zheng, W., Ye, Y.,
475 2020. Heparan sulfate assists SARS-CoV-2 in cell entry and can be targeted by approved
476 drugs in vitro. Cell Discov. 6, 80. https://doi.org/10.1038/s41421-020-00222-5
477 Zhong, L., Hu, J., Shu, W., Gao, B., Xiong, S., 2015. Epigallocatechin-3-gallate opposes HBV-
478 induced incomplete autophagy by enhancing lysosomal acidification, which is unfavorable
479 for HBV replication. Cell Death Dis. 6, e1770–e1770.
480 https://doi.org/10.1038/cddis.2015.136

481

482

483 **Figure Legends**

484 **Figure 1. EGCG pre-treatment inhibits infection by diverse CoVs. (A)** Structure of
485 epigallocatechin gallate (EGCG). **(B-C)** Pre-treatment of authentic HCoV-229E, HCoV-OC43 or
486 murine coronavirus MHV-A59 virions with EGCG for 10 min at 37°C inhibits infection of Huh7,
487 A549 or L929 cells, respectively. Mean values with standard deviation of three independent
488 experiments are plotted. **(C)** A reduction in syncytia (black arrows) was observed for EGCG-
489 treated MHV-A59. Scale bar: 200 μm. **(D)** Cell exposure to EGCG during the 2 h infection had
490 minimal effect on cell viability. Mean values with standard deviation of two independent
491 experiments with duplicates are plotted.

492

493 **Figure 2. EGCG inhibits entry of highly pathogenic CoVs and an emerging bat CoV. (A)**
494 EGCG treatment reduced entry of lentiviral particles pseudotyped with S from SARS-CoV-1,
495 MERS-CoV, SARS-CoV-2, or WIV1-CoV. Mean values with standard error of the mean of three
496 independent experiments each done in triplicates are plotted. **(B)** EGCG displayed MOI-dependent
497 inhibition of VSV-SARS-CoV-2 in Huh7, A549-ACE2 B9 and Calu-3. Mean values with standard
498 deviation of three independent experiments each in duplicates are plotted. Representative images
499 are shown. Scale bar: 200 μm.

500

501 **Figure 3. EGCG inhibits CoV attachment to cells. (A)** Pre-treatment of cells, or treatment of
502 cells post-infection with HCoV-229E or HCoV-OC43, does not inhibit infection to similar extents
503 as virion pre-treatment. Mean values with standard deviation of three independent experiments are

504 plotted. **(B)** HCoV-OC43 virions were pre-treated with EGCG or heparin for 10 min at 37°C then
505 cooled on ice and added to pre-chilled Huh7 for 1 hour on ice. **(C)** VSV-SARS-CoV-2 were pre-
506 treated as described above and added to pre-chilled Huh7 or Calu-3 cells. Attached virions were
507 quantified by RT-qPCR after washing cells with PBS three times. Mean values with standard
508 deviation from qPCR triplicates of two independent experiments are plotted.
509

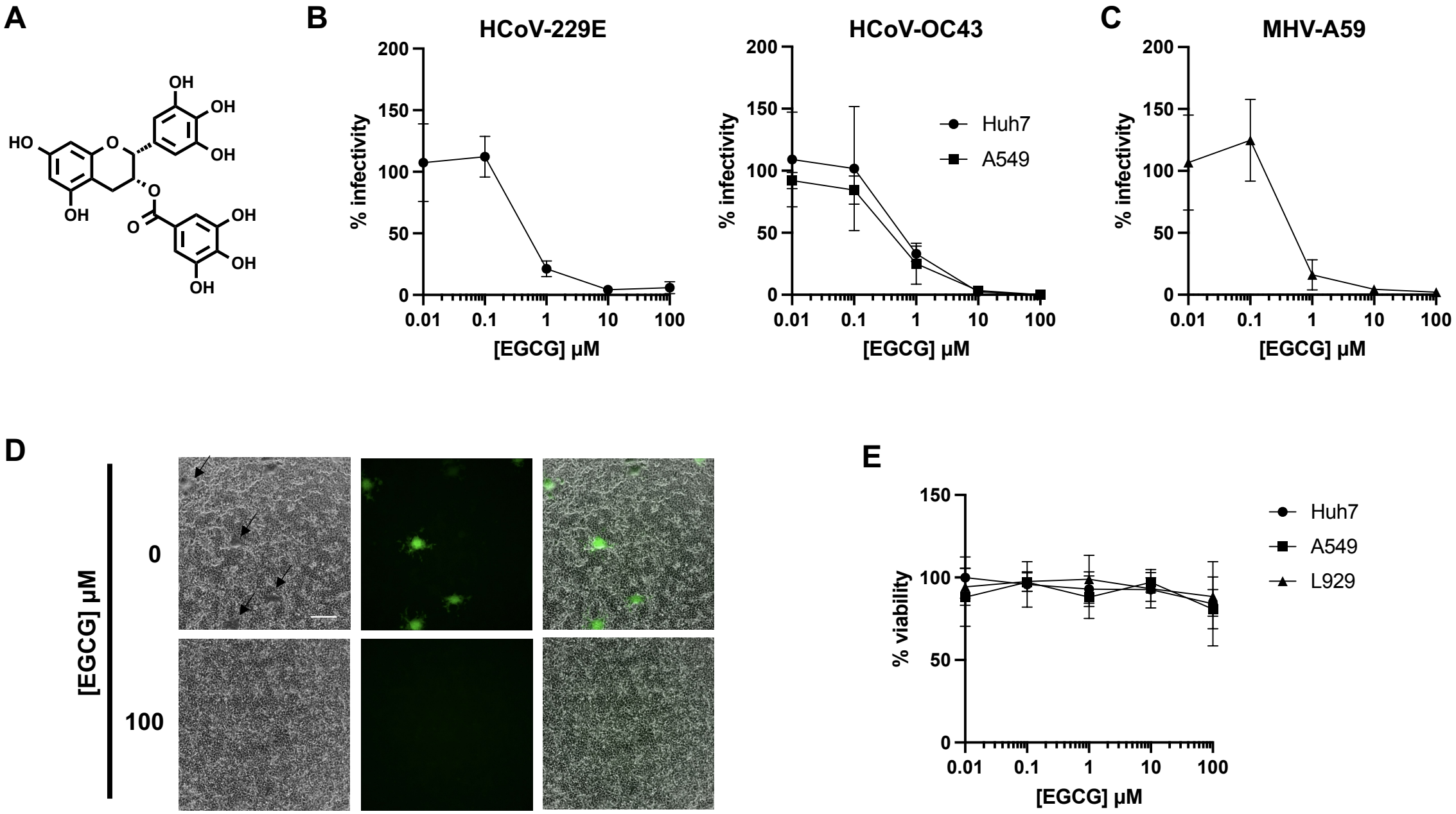
A
HO
OH
OH
OH
O
O
O
OH
OH
OH
OH
B
HCoV-229E
% infectivity
200
150
100
50
0
0.01
0.1
1
10
100
[EGCG] μM
HCoV-OC43
Huh7
A549
C
MHV-A59
D
[EGCG] μM
0
100
E
% viability
Huh7
A549
L929

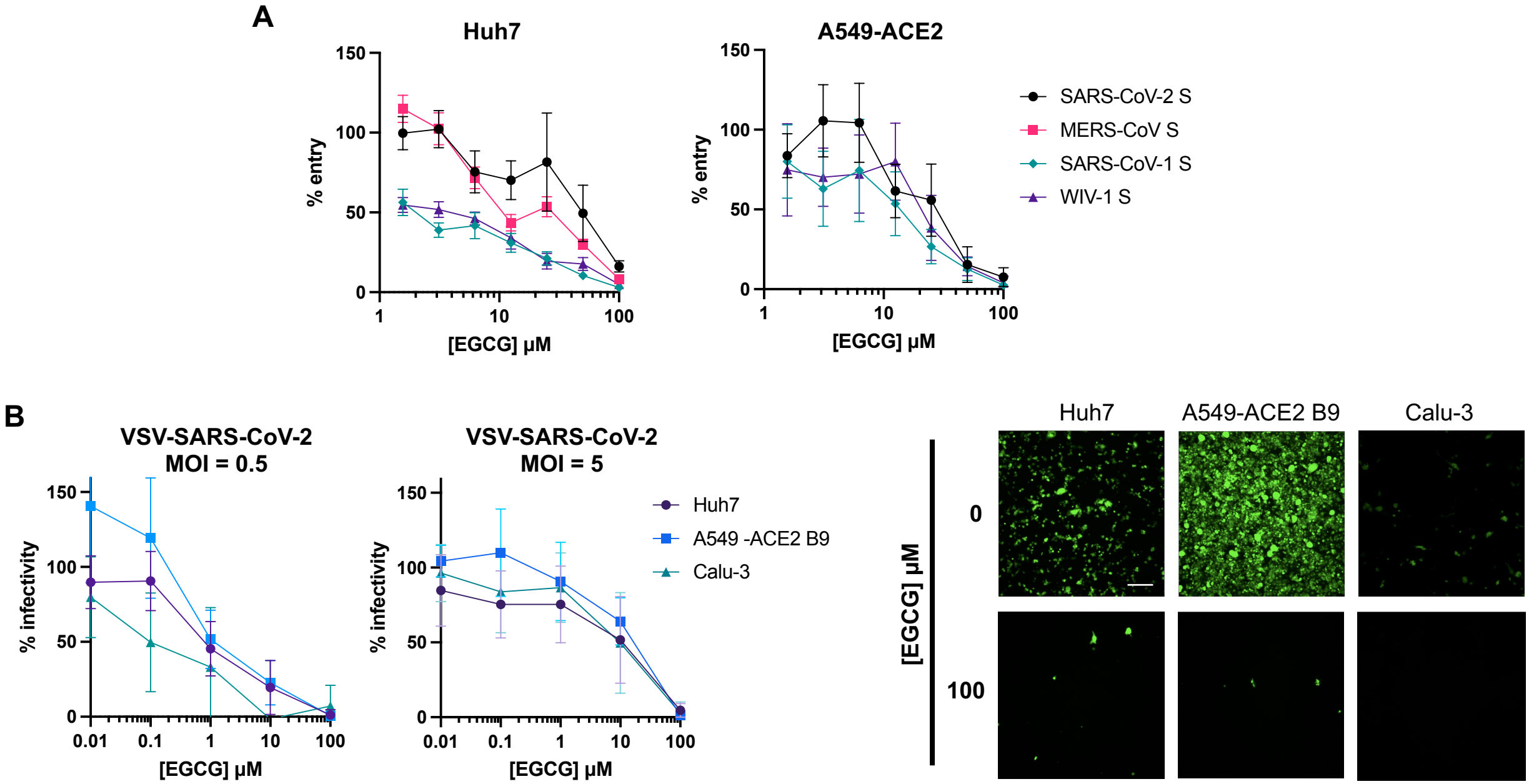
A
Huh7
A549-ACE2
% entry
150
100
50
0
1
10
100
[EGCG] μM
SARS-CoV-2 S
MERS-CoV S
SARS-CoV-1 S
WIV-1 S
B
VSV-SARS-CoV-2
MOI = 0.5
VSV-SARS-CoV-2
MOI = 5
% infectivity
0.01
0.1
Huh7
A549 -ACE2 B9
Calu-3
Huh7
A549-ACE2 B9
Calu-3
[EGCG] μM
0
100

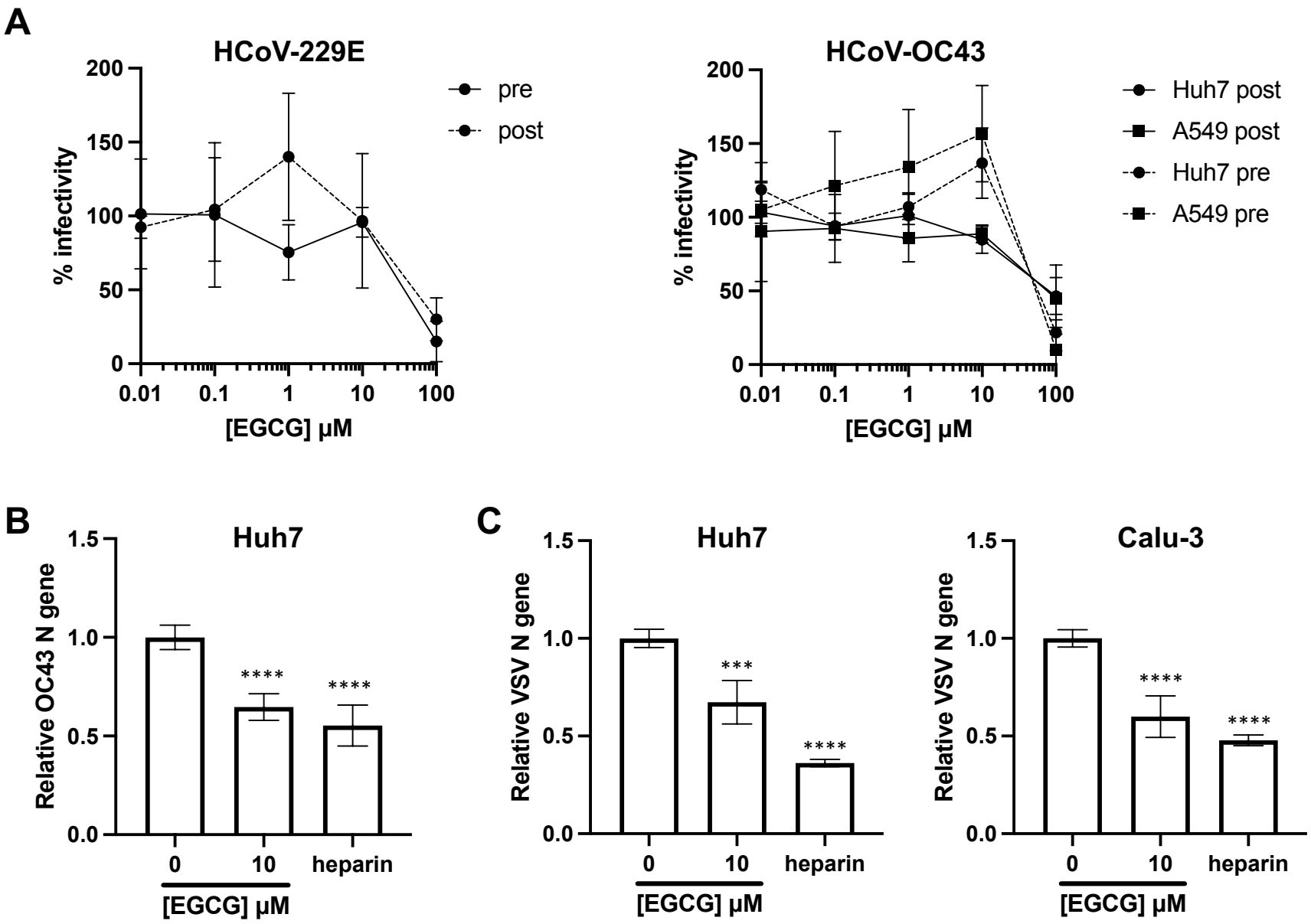
A
HCoV-229E
% infectivity
200
150
100
50
0
0.01
0.1
1
10
100
[EGCG] μM
pre
post
HCoV-OC43
% infectivity
[EGCG] μM
Huh7 post
A549 post
Huh7 pre
A549 pre
B
Huh7
Relative OC43 N gene
1.5
1.0
0.5
0.0
****
****
0
10
heparin
[EGCG] μM
C
Huh7
Relative VSV N gene
***
****
Calu-3
Relative VSV N gene
****
****